

Formation of mega-parsec giant radio sources from hosts residing in dark matter halos of different masses and with normal hot baryonic gas fractions

Xiaodong Duan^{1,2}

¹ School of Physics, Henan Normal University, Xinxiang 453007, People's Republic of China;
e-mail: duanxiaodong@htu.edu.cn

² Center for Theoretical Physics, Henan Normal University, Xinxiang 453007, People's Republic of China.

March 9, 2026

ABSTRACT

Context. Mega-parsec giant radio sources (GRSs) have been known for decades. Their known population has soared from several hundred to more than 10^4 in recent years. However, the formation mechanisms of GRSs remain elusive, and one explanation suggested is that they form in a low-density environment.

Aims. In this work, we study the formation and properties of GRSs associated with dark matter halos of different masses and normal gas density environment. This study can lay the groundwork for future observations aimed at probing the gas environment, particularly the baryonic gas fraction, in the host dark matter halos of GRSs.

Methods. We use magnetohydrodynamic simulations to study the formation of GRSs from hosts residing in dark matter halos with masses of 10^{13} , 10^{14} and 10^{15} solar masses, adopting normal hot baryonic gas fractions (0.02, 0.05, and 0.1). We inject jet energy of 0.06 percent of the central black hole's relativistic energy in their host galaxies with power of 0.05 percent of the Eddington luminosity.

Results. The successful formation of GRSs from hosts in all three dark matter halos with normal hot baryonic gas fractions indicates that an unusual low-density gas environment is not a necessary condition for their formation. The jetted lobe growing from hosts in dark matter halo of 10^{13} solar masses exhibits a wider shape than those in dark matter halos of 10^{14} and 10^{15} solar masses. The evolution of the simulated GRSs in the radio power-linear size diagram shows that their radio power can reach values comparable to observational data at similar physical scales. Furthermore, the radio power typically increases with dark matter halo mass. When we simulate a higher-power jet in a lower-mass dark matter halo, the results reveal a deviation from the simple linear relation between jet power and radio luminosity.

Key words. Galaxies: active – Galaxies: jets – Radio continuum: galaxies – Magnetohydrodynamics

1. Introduction

Giant radio sources (GRSs), defined as those exceeding 0.7 Mpc in size and including giant radio galaxies (GRGs) and quasars (GRQs), have been known for a long time (Willis et al. 1974; Dabhade et al. 2023). The number of known GRSs has soared from several hundred to more than 10^4 , and the size record has been updated to approximately 7 Mpc in recent years (Dabhade et al. 2023; Mostert et al. 2024; Oei et al. 2024a). The feedback from GRSs may be important for galaxy evolution (Sorini et al. 2022; Cen 2024; Qiu & Cen 2025). However, the formation mechanism of these mega-parsec GRSs remains unclear.

Several mechanisms, including a low-density environment, unusually high jet power, and recurrent jet activity, have been proposed to explain the formation of GRSs (Dabhade et al. 2023). Recently, magnetohydrodynamic simulations have been applied to study the formation of GRSs (Duan et al. 2025; Giri et al. 2025a,b). Duan et al. (2025) found that energetic, low-power (but long-lasting), continuous jets endowed with significant toroidal magnetic fields facilitate the formation of GRSs in cluster environments, while the faintness of GRSs with even lower jet power may render them unobservable. Giri et al. (2025a) and Giri et al. (2025b) show that Mpc scale radio sources formed in all of their simulations, which varied in jet power and

ambient environment (e.g., the location of the jet base in a tri-axial medium). This suggests that GRSs may be more common than previously believed.

The low-density environment is the most widely invoked explanation for the formation of GRSs (Chen et al. 2011; Dabhade et al. 2020b; Lan & Prochaska 2021; Oei et al. 2024b). By adopting the optical velocity dispersion of group members within 0.7 Mpc of GRG NGC 6251, Chen et al. (2011) indirectly suggested that the density of X-ray emitting gas in NGC 6251 is unusually low. Recent observations indicate that GRSs can form in a wide variety of cosmic environments (Oei et al. 2024a,b). However, these observations have not directly related GRSs to the local gas environment through which the jets propagate, while strong jet–ambient gas interactions will suppress the growth of large-scale lobes (Duan et al. 2025). Besides the interstellar medium (ISM), the gas environment of the hosts primarily consists of hot circumgalactic medium (CGM) within the dark matter halos for hosts as massive galaxies (Tumlinson et al. 2017), and of intragroup or intracluster medium for hosts as central giant elliptical galaxies in the galaxy groups or clusters (Fabian 2012). The massive satellites could also retain hot CGM (Rohr et al. 2024; Zhang et al. 2024). The amount of hot gas in a dark matter halo is characterized by its hot baryonic gas fraction, which

for low-redshift galaxies primarily depends on the mass of dark matter halo (Xu et al. 2020; Dev et al. 2024). In this study, we use numerical simulations to investigate whether forming GRSs requires a low-density gas environment (i.e., a low baryonic gas fraction) within dark matter halos of varying masses. The results could be checked by future observations aimed at probing the gas environment, particularly the baryonic gas fraction, in the host dark matter halos of GRSs.

This letter is structured as follows. In Sect. 2, we describe the basic methodology. In Sect. 3, we present an investigation of GRS formation in galaxies with varying masses and hot gas baryonic fractions. Finally, in Sect. 4, we summarize the key findings.

2. Methods

2.1. Numerical setup

Following Duan et al. (2025), we solve the ideal magnetohydrodynamic (MHD) equations numerically in 2.5-dimensional cylindrical coordinates using MPI-AMRVAC 2.0 (Xia et al. 2018). The numerical schemes and boundary conditions adopted in this work are the same as those in Duan et al. (2025). We simulate only one side of the bipolar jets. The computational domain is initially refined with different spatial resolutions: 0.25 kpc within 100 kpc, 0.5 kpc from 100 to 200 kpc, 1 kpc from 200 to 400 kpc, and 2 kpc from 400 kpc to the outer boundary. The outer boundaries are set at 800 kpc, 1000 kpc, and 2000 kpc for the dark matter halos with virial radius of 416 kpc, 896 kpc and 1931 kpc, respectively.

2.2. Galaxy model

The galaxy model in this work is similar to the approach of Duan et al. (2025), and the only difference lies in the concentration parameter, which we relate to redshift (Schneider 2015) as

$$C \approx 6.7 \left(\frac{M_{\text{vir}}}{2 \times 10^{12} h M_{\odot}} \right)^{-0.1} (1+z)^{-0.5}, \quad (1)$$

where M_{vir} is the virial mass of the dark matter halo. We adopt the scaled Hubble constant $h = 0.7$ and redshift $z = 0.2$ in this work. The main input galaxy parameters are M_{vir} and the hot gas fraction f_g (the ratio of hot baryonic gas mass to M_{vir}). Following recent observations of Dev et al. (2024), we adopt hot gas fractions f_g of 0.02, 0.05, and 0.1 for M_{vir} of 10^{13} , 10^{14} and 10^{15} solar masses, respectively. This indicates that we are considering typical, rather than unusual, hot gas fractions. The gas density, temperature, and pressure profiles are illustrated in Fig. A.1. While the remaining parameters, including the stellar mass and supermassive black hole mass of the central host, depend on the virial mass of the dark matter halo. These parameters are listed in Table 1.

2.3. Jet injection

To establish reasonable values for the jet energy and power, we provide some estimates in this section. Assuming that the jet energy is extracted from the spin of the black hole, it can be estimated from the black hole's rotational energy (Meier 2012):

$$E_{\text{rot}} = \left(1 - \sqrt{\frac{1 + \sqrt{1 - a^2}}{2}} \right) M_{\text{bh}} c^2, \quad (2)$$

where a is the black hole spin parameter, M_{bh} is the black hole mass, and c is the speed of light. As indicated by observations (Dabhade et al. 2020a), we consider black holes with a low spin parameter of $a \lesssim 0.1$. The corresponding typical rotational energy is $\lesssim 1.3 \times 10^{-2} M_{\text{bh}} c^2$.

The jet power can be related to the black hole accretion rate as

$$P_{\text{jet}} = \eta_{\text{jet}} \dot{M}_{\text{bh}} c^2, \quad (3)$$

where η_{jet} is the jet efficiency. The luminosity of the accretion flow is given by

$$L = \eta_{\gamma} \dot{M}_{\text{bh}} c^2, \quad (4)$$

where η_{γ} is the radiative efficiency. The Eddington ratio is $\lambda_{\text{Edd}} = L/L_{\text{Edd}}$, where L_{Edd} is the Eddington luminosity. The ratio of jet power to Eddington luminosity is $\lambda_{\text{jet}} = P_{\text{jet}}/L_{\text{Edd}}$. Combining these relations yields

$$\lambda_{\text{jet}} = \lambda_{\text{Edd}} \frac{\eta_{\text{jet}}}{\eta_{\gamma}}. \quad (5)$$

Jets can be launched when black holes are in sub-Eddington hot accretion or super-Eddington accretion states (Tchekhovskoy 2015). For a hot accretion flow, the upper limit of Eddington ratio λ_{Edd} is about 2% (Yuan et al. 2018). When the hot accretion flow is magnetically arrested, the maximum radiative efficiency $\eta_{\gamma} \approx 0.08$ (Xie & Zdziarski 2019). The jet efficiency $\eta_{\text{jet}} \lesssim 1.3a^2 \lesssim 1.3\%$ for low-spin black holes with $a \lesssim 0.1$ (Davis & Tchekhovskoy 2020). This gives the ratio of jet power to Eddington luminosity $\lambda_{\text{jet}} \lesssim 3.3 \times 10^{-3}$. The values of jet energy and power in all our runs are shown in Table 1. We note that the adopted jet power $P_{\text{jet}} \lesssim 10^{44} \text{ erg s}^{-1}$ is consistent with observational results for central black holes in GRSs with low spin ($a < 0.1$) and masses of $10^8 - 10^9 M_{\odot}$ (Dabhade et al. 2020a).

In this work, we initialize the jets in all runs with a magnetic energy fraction f_m of 0.8, a kinetic energy fraction f_k of 0.05, and a thermal energy fraction f_{th} of 0.05. The jets are activated at the start of the simulation with a constant power during the active phase (when $t \leq t_{\text{jet}}$). Throughout this phase, mass, momentum, and non-magnetic energy are injected into a cylindrical region centered on the origin. This region has a cross-sectional radius of $R_0 = 1$ kpc and extends 1 kpc along the $+z$ axis. The jet velocity is set to a constant value of $0.1c$. The parameter governing the magnetic field configuration, α_p , is set to 0.3 for all runs, indicating that the injected magnetic field is dominated by the toroidal component. Further details of the magnetic field injection method can be found in Appendix B of Duan et al. (2025). The impacts of the jet parameters are summarized in Appendix B.

3. Results and discussion

3.1. Evolution of scale and morphology

The scale evolution of the radio sources in our four runs is shown in the top panel of Fig. 1. As shown, all four radio sources grow to become GRSs ($2r_h > 0.7$ Mpc) within the jet duration ($t_{\text{jet}} = 540$ Myr, indicated by the dotted vertical line). Given the normal values adopted for the hot gas fraction and the reasonable jet energy and power (Sects. 2.2 and 2.3), the formation of GRSs in these runs indicates that an unusually low-density gas environment is not necessary for GRS formation. The jetted lobes in runs M13 and M14 propagate beyond the virial radius

Table 1. Parameters of Our Simulations

Run	M_{vir}/M_{\odot}	f_g	M_{\star}/M_{\odot}	M_{bh}/M_{\odot}	$E_{\text{jet}}(\text{erg})$	$E_{\text{jet}}/M_{\text{bh}}c^2$	$R_{\text{fb}}(\text{kpc})$	$P_{\text{jet}}(\text{erg s}^{-1})$	$P_{\text{jet}}/L_{\text{Edd}}$
M13	10^{13}	0.02	1.20×10^{11}	1.96×10^8	2.2×10^{59}	6.2×10^{-4}	285	1.27×10^{43}	5×10^{-4}
M14	10^{14}	0.05	2.84×10^{11}	5.16×10^8	5.8×10^{59}	—	62	3.35×10^{43}	—
M15	10^{15}	0.1	6.58×10^{11}	1.32×10^9	1.5×10^{60}	—	34	8.57×10^{43}	—
M14E1	10^{14}	0.05	2.84×10^{11}	5.16×10^8	2.9×10^{60}	3.1×10^{-3}	139	1.67×10^{44}	2.5×10^{-3}

Notes. The parameters for the galaxies and jets in our simulations. The parameters encompass virial mass of the dark matter halo M_{vir} , hot gas fraction f_g , stellar mass of central host M_{\star} , black hole mass M_{bh}/M_{\odot} , jet energy E_{jet} , ratio of jet energy to relativistic energy of the black hole $E_{\text{jet}}/E_{\text{bh}}$, characteristic feedback radius R_{fb} , jet power P_{jet} , and ratio of jet power to Eddington luminosity $P_{\text{jet}}/L_{\text{Edd}}$. A fixed jet active duration of $t_{\text{jet}} = 548$ Myr is adopted for all runs. The symbol "—" indicates that the corresponding parameter shares the same value as the one immediately above it.

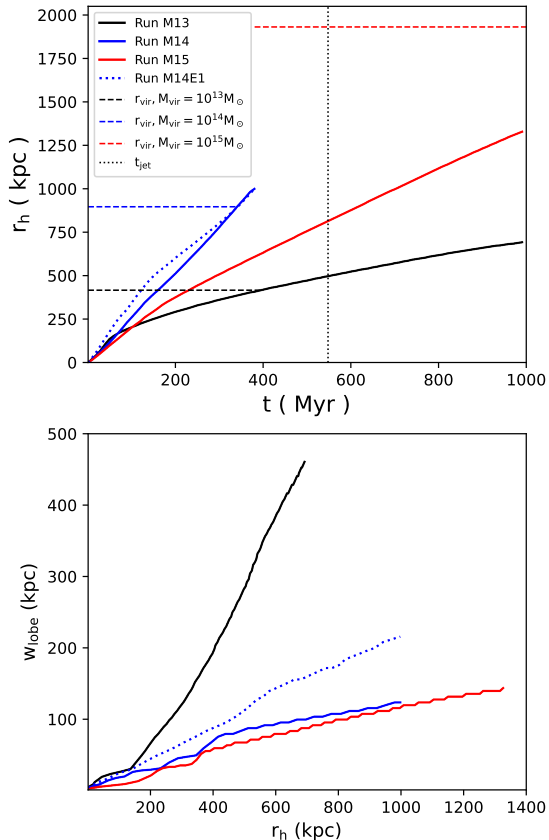


Fig. 1. Evolution of the traveling distance r_h of the bubble heads (one-sided scale of the GRSs, top panel) and the lobe width w_{lobe} varying with r_h (bottom panel). The vertical dotted lines in the top panel indicate the times when the jets are shut off, while the horizontal dashed lines denote the virial radius of the dark matter halos. Different line colors represent different dark matter halo masses.

(marked by horizontal dashed lines), while the lobes in run M15 have not reached the virial radius by the end of the simulation ($t = 1$ Gyr, indicated by the vertical dotted line). Since the jets are injected with the same fraction of the black hole’s relativistic energy and the same ratio of jet power to Eddington luminosity ($E_{\text{jet}}/M_{\text{bh}}c^2$ and $P_{\text{jet}}/L_{\text{Edd}}$ in Table 1) in runs M13, M14, and M15, the fastest lobe propagation in run M14 suggests that GRSs form more readily from hosts in $10^{14}M_{\odot}$ dark matter halos than in 10^{13} or $10^{15}M_{\odot}$ halos.

The morphology of the jetted lobes shows significant differences between the runs. The widths of the lobes as a function of length are shown in the bottom panel of Fig. 1. As can be seen, the jetted lobe in run M13 is much wider than those in runs M14

and M15, as also shown in Fig. B.1. This suggests that it is easier to form GRSs with wider shapes from hosts in lower-mass dark matter halos, where they experience more adiabatic cooling in the lower-pressure environment. The very slim lobe formed in run M15, which has a denser gas environment and indicates that a dense gas environment may help collimate the jetted lobes. On the other hand, the morphology of the lobes is also related to the jet energy. When the jet energy is increased in run M14E1, the lobe shows a wider shape compared to run M14 (see the blue dotted line in the bottom panel of Fig. 1 and the right panel of Fig. B.1).

The dependence of lobe morphology on both the environment and jet energy can be characterized by the characteristic feedback radius R_{fb} , defined as the radius within which the initial thermal energy of the ambient gas equals the jet outburst energy (Duan & Guo 2020). The values of R_{fb} for all runs are listed in Tab. 1. As can be seen, the R_{fb} value for run M13 is significantly larger than those for runs M14 and M15, despite the lower jet energy in run M13.

3.2. P-D diagram

The radio power-linear size diagram (P-D diagram) is an important diagnostic for studying radio sources with different jet powers (Baldwin 1982; Hardcastle 2018). In this work, we calculate the radio power (or radio luminosity) using the same method as Duan et al. (2025). The evolution of the GRSs in our four runs (set at redshift $z = 0.2$) in the P-D diagram, together with observed GRSs selected within the redshift range $0.1 < z < 0.3$, is shown in the top panel of Fig. 2. As shown, the radio powers of the GRSs in our simulations are comparable to those observed at similar scales. Comparing the radio powers of the jetted lobes in runs M13, M14, and M15, we find that the radio power of GRSs generally increases with dark matter halo mass (and consequently with jet energy and power).

The linear relation between jet power and radio power is widely used in the literature (Hardcastle 2018; Dabhade et al. 2020a; Ye et al. 2025). In our simulations, although the jet power in run M14E1 is higher than in M15, the radio power of the lobe in run M14E1 is lower than that in run M15 as they evolve from approximately 250 kpc to 1600 kpc (top panel of Fig. 2). This indicates a deviation from the simple linear relation between jet power and radio power. We show the relationship between jet power and radio power at three characteristic scales (50 kpc, 800 kpc, and 1200 kpc) in the bottom panel of Fig. 2. In reality, the radio power of jets should depend on the galactic environment, jet power, and the evolutionary stage at which they are observed, making the relationship considerably more complex than a simple linear correlation.

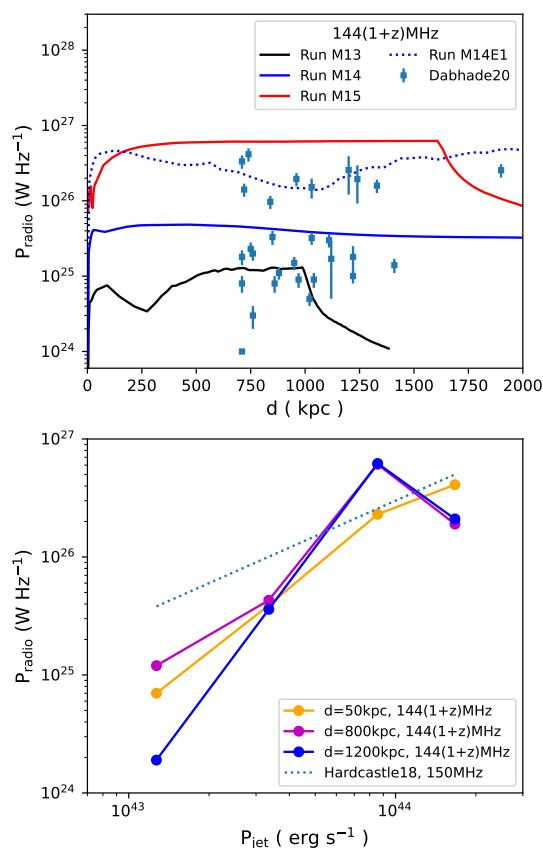


Fig. 2. Evolution of the simulated radio sources in the P-D diagram (top panel) and the relation between power and radio power (luminosity) of jets at three typical scales (50kpc, 800kpc and 1200kpc) of radio sources (bottom panel). In top panel, different line colors represent different masses of dark matter halos. The radio power is calculated at $144(1+z)$ MHz, where we adopt redshift $z = 0.2$. The data points utilized in this analysis are sourced from [Dabhade et al. \(2020b\)](#) with in the redshift range $0.1 < z < 0.3$. In bottom panel, different line colors represent different scales of the simulated radio sources plotted in the top panel. The dotted line show the linear related given by [Hardcastle \(2018\)](#): $P_{\text{radio}}(150\text{MHz}) = 3 \times 10^{27} (P_{\text{jet}}/10^{38}\text{W}) \text{WHz}^{-1}$.

4. Conclusions

We use MHD simulations to study the formation of GRSs from central galaxies in dark matter halos of 10^{13} , 10^{14} , and $10^{15} M_{\odot}$, assuming normal hot gas fractions of 0.02, 0.05, and 0.1. The main results are:

(i) GRSs form in all three halo masses when jets are injected with energy $\sim 0.06\%$ of the central black hole's relativistic energy and power $\sim 0.05\%$ of the Eddington luminosity. This shows that an unusually low-density environment is not necessary for GRS formation. With these fixed energy and power ratios, lobe propagation is fastest in the $10^{14} M_{\odot}$ halo, indicating that GRS formation is most efficient in this mass range.

(ii) Lobe morphology differs significantly across dark matter halo masses. Lobes in the $10^{13} M_{\odot}$ dark matter halo are much wider than in higher-mass halos, suggesting that wider GRSs form more easily in lower-mass dark matter halos due to enhanced adiabatic cooling in the lower-pressure environment. The dependence of lobe shape on the ambient environment and jet energy is characterized by the feedback radius R_{fb} , with larger R_{fb} corresponding to broader lobes.

(iii) In the P-D diagram, the simulated GRSs reach radio powers comparable to observed GRSs at similar sizes, with ra-

dio power generally increasing with dark matter halo mass. For higher-power jets in lower-mass halos, the results show a deviation from a simple linear relation between jet power and radio luminosity.

Acknowledgements. This work was supported by the High Performance Computing Center of Henan Normal University.

References

- Baldwin, J. E. 1982, in IAU Symposium, Vol. 97, Extragalactic Radio Sources, ed. D. S. Heeschen & C. M. Wade, 21–24
- Cen, R. 2024, Proceedings of the National Academy of Science, 121, e2402435121
- Chen, R., Peng, B., Strom, R. G., & Wei, J. 2011, MNRAS, 412, 2433
- Chen, Y.-H., Heinz, S., & Hooper, E. 2023, MNRAS, 522, 2850
- Dabhade, P., Mahato, M., Bagchi, J., et al. 2020a, A&A, 642, A153
- Dabhade, P., Röttgering, H. J. A., Bagchi, J., et al. 2020b, A&A, 635, A5
- Dabhade, P., Saikia, D. J., & Mahato, M. 2023, Journal of Astrophysics and Astronomy, 44, 13
- Davis, S. W. & Tchekhovskoy, A. 2020, ARA&A, 58, 407
- Dev, A., Driver, S. P., Meyer, M., et al. 2024, MNRAS, 535, 2357
- Duan, X. & Guo, F. 2020, ApJ, 896, 114
- Duan, X., Wu, L., Zhang, R., & Li, J. 2025, A&A, 697, A147
- Fabian, A. C. 2012, ARA&A, 50, 455
- Fang, X.-E., Guo, F., & Yuan, Y.-F. 2020, ApJ, 894, 1
- Gan, Z., Li, H., Li, S., & Yuan, F. 2017, ApJ, 839, 14
- Giri, G., Bagchi, J., Thorat, K., et al. 2025a, A&A, 693, A77
- Giri, G., Fendt, C., Bagchi, J., et al. 2025b, arXiv e-prints, arXiv:2510.03037
- Guo, F. & Mathews, W. G. 2014, ApJ, 780, 126
- Guo, F., Zhang, R., & Fang, X.-E. 2020, ApJ, 904, L14
- Hardcastle, M. J. 2018, MNRAS, 475, 2768
- Hardcastle, M. J. & Croston, J. H. 2020, New A Rev., 88, 101539
- Lan, T.-W. & Prochaska, J. X. 2021, MNRAS, 502, 5104
- Meier, D. L. 2012, Black Hole Astrophysics: The Engine Paradigm (Berlin, Heidelberg: Springer Berlin Heidelberg)
- Mignone, A., Rossi, P., Bodo, G., Ferrari, A., & Massaglia, S. 2010, MNRAS, 402, 7
- Mostert, R. I. J., Oei, M. S. S. L., Barkus, B., et al. 2024, A&A, 691, A185
- Oei, M. S. S. L., Hardcastle, M. J., Timmerman, R., et al. 2024a, Nature, 633, 537
- Oei, M. S. S. L., van Weeren, R. J., Hardcastle, M. J., et al. 2024b, A&A, 686, A137
- Qiu, Y. & Cen, R. 2025, Proceedings of the National Academy of Science, 122, e2506790122
- Rohr, E., Pillepich, A., Nelson, D., Ayromlou, M., & Zinger, E. 2024, A&A, 686, A86
- Schneider, P. 2015, Extragalactic Astronomy and Cosmology: An Introduction (Berlin, Heidelberg: Springer Berlin Heidelberg)
- Sorini, D., Davé, R., Cui, W., & Appleby, S. 2022, MNRAS, 516, 883
- Tchekhovskoy, A. 2015, in Astrophysics and Space Science Library, Vol. 414, The Formation and Disruption of Black Hole Jets, ed. I. Contopoulos, D. Gabuzda, & N. Kylafis, 45
- Tumlinson, J., Peeples, M. S., & Werk, J. K. 2017, ARA&A, 55, 389
- Willis, A. G., Strom, R. G., & Wilson, A. S. 1974, Nature, 250, 625
- Xia, C., Teunissen, J., El Mellah, I., Chané, E., & Keppens, R. 2018, ApJS, 234, 30
- Xie, F.-G. & Zdziarski, A. A. 2019, ApJ, 887, 167
- Xu, W., Guo, Q., Zheng, H., et al. 2020, MNRAS, 498, 1839
- Ye, X.-H., Baldi, R. D., Chen, Y.-Y., Bastieri, D., & Fan, J.-H. 2025, A&A, 697, A176
- Yuan, F. & Narayan, R. 2014, ARA&A, 52, 529
- Yuan, F., Yoon, D., Li, Y.-P., et al. 2018, ApJ, 857, 121
- Zhang, Y., Comparat, J., Ponti, G., et al. 2024, A&A, 690, A267

Appendix A: Gas profile

In this appendix, we present in Fig. A.1 the radial profiles of electron number density, temperature, and thermal pressure for dark matter halos of virial masses 10^{13} , 10^{14} , and $10^{15} M_{\odot}$. The gas model is modified from Fang et al. (2020) and Guo et al. (2020) as shown in Duan et al. (2025). For comparison, profiles corresponding to hot gas fractions lower than the adopted normal value are shown as dotted lines. These illustrate that lower hot gas fractions result in clearly lower pressure profiles. A comparison of our model with the observed profiles of galaxy cluster A1795 with similar virial mass can be found in Appendix A of Duan et al. (2025). The profiles in Fig. A.1 can also be compared with the gas profiles compiled by Guo & Mathews (2014) for dark matter halos of comparable mass. The overall magnitude shows good agreement at radii beyond ~ 10 kpc, whereas data in the halo cores are typically absent or have large uncertainties.

Appendix B: Impact of jet set-up

The composition of active galactic nucleus jets remains an unsolved problem (Hardcastle & Croston 2020), and the accretion state of the central black holes in GRS host galaxies is also unclear. Furthermore, different jet formation models (e.g., the Blandford-Znajek, Blandford-Payne, and magnetic tower models) predict different jet compositions (Yuan & Narayan 2014). Therefore, a careful consideration of jet parameters is essential when simulating jet feedback processes. A study of key jet parameters — such as power, energy composition, and magnetic field structure for the GRS jets, has been presented by Duan et al. (2025).

We briefly summarize the impact of jet parameters as follows:

(i) The most significant parameter is the jet power, which exhibits a "lower power-larger bubble" effect: for a fixed total energy, lower-power jets tend to produce larger radio sources. This occurs primarily because high-power jets are injected with higher internal pressure, causing them to expand laterally and penetrate less deeply into the ambient atmosphere. Additionally, higher-power jets dissipate their energy more rapidly in the early stages via adiabatic losses.

(ii) The magnetic field structure also has a significant impact: strong poloidal fields hinder radio lobe growth, a result also reported by Chen et al. (2023). The influence of the energy composition is less pronounced than that of jet power or magnetic field structure. However, jets dominated by toroidal magnetic field energy tend to produce larger radio sources than those dominated by kinetic or thermal energy.

(iii) While all simulated low-power jets ($10^{-4} - 10^{-3} L_{\text{Edd}}$) from low-spin black holes can produce GRS-scale (> 0.7 Mpc) sources, jets initially dominated by kinetic, thermal, or poloidal magnetic field energy produce fainter lobes than those initially dominated by toroidal magnetic field energy. Analysis of the P–D diagram shows that jets initially dominated by toroidal magnetic field energy yield radio sources that best match current observations, though kinetically dominated jets also fall within the observational region.

On the other hand, Gan et al. (2017) found that a head–tail radio morphology is well reproduced by using a magnetic energy dominant jet model, whereas lobes from jets injected with kinetic or thermal energy dominance could not survive the disruptive effects of the intracluster weather. Based on these findings, we have chosen in this work to simulate jets that are injected with low power and with toroidal magnetic field energy

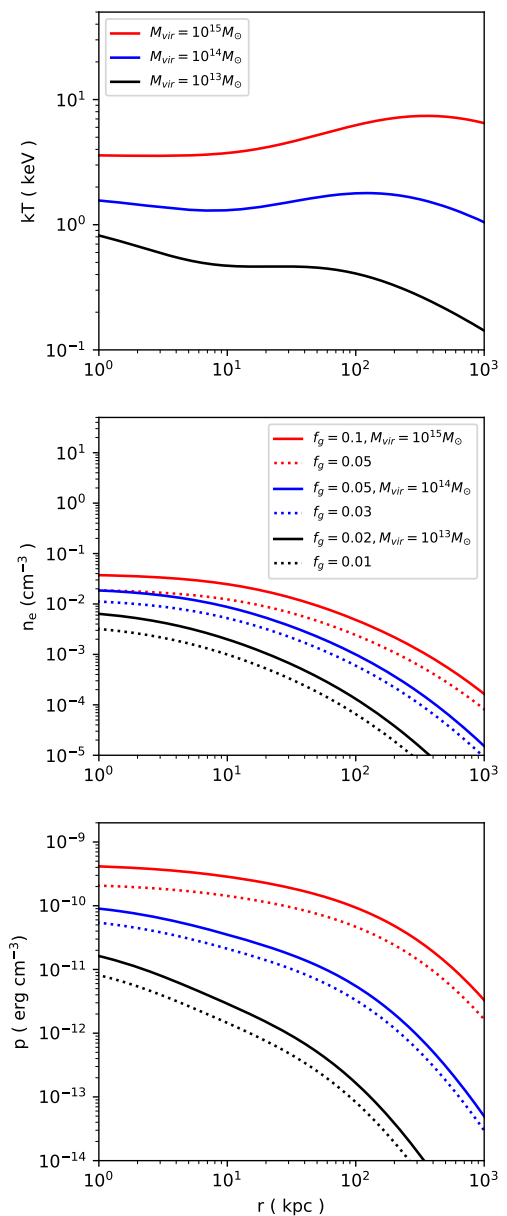


Fig. A.1. Profiles of electron number density, temperature, and pressure for dark matter halos of virial mass (M_{vir}) 10^{13} (black), 10^{14} (blue), and 10^{15} (red) solar masses. The dotted lines for density and pressure correspond to hot gas fractions (f_g) lower than the adopted normal value. The temperature profiles are independent of the gas fraction in our model. Profiles outside the virial radius are fitted as extensions of the inner profiles.

as the dominant component. We also note that, even when jets are initially injected with magnetically dominated energy, their lobes become dominated by kinetic and thermal energy as they evolve to larger scales from the host galaxy center, as shown in Figure C.1 of Duan et al. (2025).

Another factor influencing the properties of simulated GRSs is the dimensionality of the simulations, as discussed in Duan et al. (2025). For jets injected with magnetically dominated energy, the two-dimensional axisymmetric MHD setup used here can suppress certain MHD instabilities—notably the kink instability—that would develop in full three-dimensional simulations (Mignone et al. 2010). The kink instability triggers non-axisymmetric features such as jet wiggling, which cannot be captured in our axisymmetric simulations. However, our focus

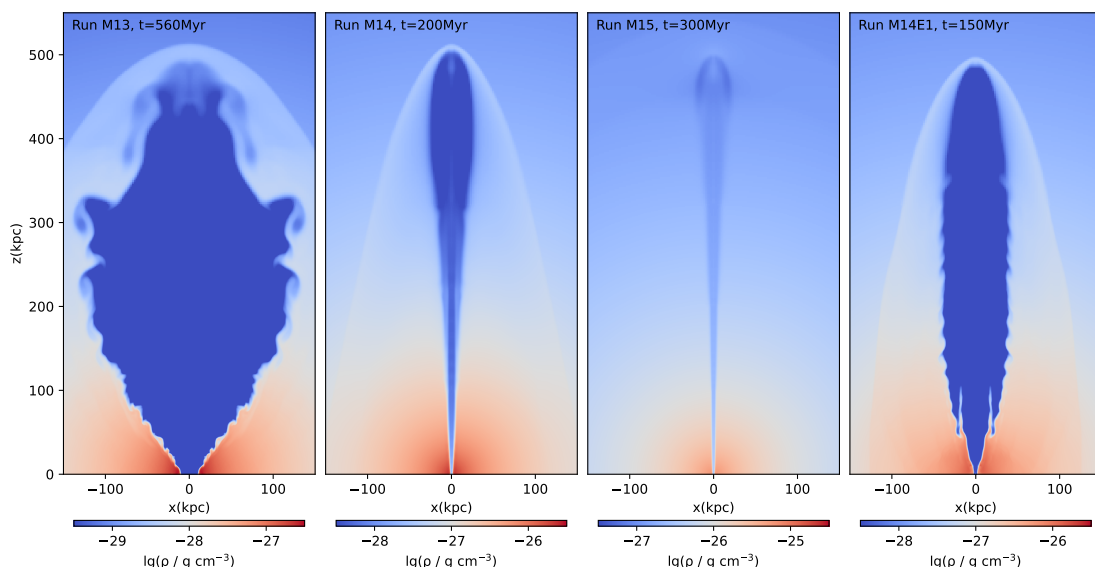


Fig. B.1. Snapshots of the density distribution for our four runs, captured when the bipolar radio lobes reach a scale of about 1 Mpc.

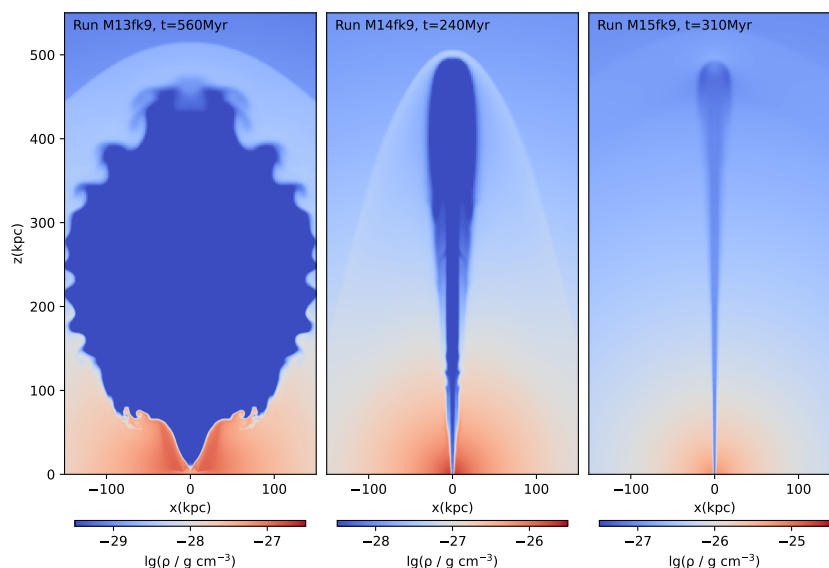


Fig. B.2. Density snapshots for runs of jets injected with kinetic energy dominant, taken when the bipolar lobes reach ~ 1 Mpc. The runs M13fk9, M14fk9, and M15fk9 differ from M13, M14, and M15 solely in their injected energy fractions: $f_k = 0.9$ (kinetic), $f_m = 0.05$ (magnetic), and $f_{th} = 0.05$ (thermal).

is not on the detailed morphology of the jet lobes but primarily on their final spatial extent. Importantly, the overall lobe scale remains similar in axisymmetric and three-dimensional MHD simulations, as demonstrated by [Mignone et al. \(2010\)](#). Furthermore, jets injected with kinetically dominated energy can also produce mega-parsec-scale sources, though they may require a longer time as can be seen by comparing the left three panels of [Fig. B.1](#) with those in [Fig. B.2](#). [Giri et al. \(2025a\)](#) conducted three-dimensional MHD simulations of GRSs, in which the kink instability is not prominently observed. This may be because the magnetic energy fraction in their injected jets is not sufficiently high. On the other hand, the focus of their model design differs from ours. A key distinction is that [Giri et al. \(2025a\)](#) does not focus on the relationship between the jet model and the properties of the host galaxies, which is a central topic in our work. In our model, the masses of the dark matter halo, the central galaxy, and its supermassive black hole are tied together self-consistently for varying halo masses. Critical aspects such as the

gaseous atmosphere of the host—notably the hot baryonic gas fraction—are informed by observational data from dark matter halos of similar mass. Additionally, the parameters governing jet energy and power are scaled according to standard accretion physics and the available energy budget of the central black hole.